RSC Advances

PAPER

View Article Online
View Journal | View Issue

Cite this: *RSC Adv.*, 2024, **14**, 1984

Multilayer immobilizing of denitrifying *Bacillus* sp. and TiO_2–AgNPs on floating expanded clay carrier for co-treatment of nitrite and pathogens in aquaculture†

Phuong Ha Hoang,‡[ab] Minh Thi Nguyen,‡[ab] Ke Son Phan,[ac] Huong Giang Bui,[ab] Thi Thu Huong Le,[d] Nhat Huy Chu,[ab] Ngoc Anh Ho,[ab] Quang Huy Pham,[b] Xuan Khoi Tran[b] and Phuong Thu Ha *[ac]

Nitrite contamination and the spread of pathogens can seriously degrade water quality. To simultaneously control these factors, an innovative approach of fabricating a remediation agent that contained denitrifying bacteria and TiO_2–AgNPs co-immobilized on floating expanded clay (EC) was proposed in this study. The EC was fabricated from a mixture of clay and rice husk through pyrolysis at a high temperature of 1200 °C, followed by a rapid cooling step to create a porous structure for the material. TiO_2NPs were modified with Ag to shift the absorbance threshold of TiO_2–AgNPs into the visible region of 700–800 nm. The experimental results showed that the stirring speed of 250 rpm was suitable for immobilizing TiO_2–AgNPs on EC and achieved the highest Ti and Ag content of 639.38 ± 3.04 and 200.51 ± 3.71 ppm, respectively. Coating TiO_2–Ag/EC with chitosan (0.5%) significantly reduced the detachment level of immobilized TiO_2–AgNPs compared to that of the material with no coating. In particular, this functionalized material inhibited 99.93 ± 0.1% of *Vibrio parahaemolyticus* pathogen but did not adversely affect the denitrifying bacteria after 2 h of visible light irradiation. Based on the electrostatic bond between oppositely charged polymers, the denitrifying bacteria, *Bacillus* sp., in alginate solution was successfully immobilized on the chitosan-coated TiO_2–Ag/EC with a bacteria density of (76.67 ± 9.43) × 10^7 CFU g^{-1}, retaining its nitrite removal efficiency at 99.0 ± 0.27% through six treatment cycles. These findings provide solid evidence for further investigating the combination of biodegradation and photodegradation in wastewater treatment.

Received 29th October 2023
Accepted 11th December 2023

DOI: 10.1039/d3ra07361k

rsc.li/rsc-advances

Introduction

In aquaculture, disease outbreaks are inevitable environmental factors that affect the growth of fish and shellfish.[1] Numerous studies have identified that acute hepatopancreatic necrosis disease (AHPND), caused by *Vibrio* spp., is the most serious infectious disease threat to shrimp farmers in the region. Multiple species of shrimp, such as *L. vannamei*, *P. monodon*, *M. rosenbergii*, and *Artemia franciscana*, are reported to be susceptible to AHPND in the early stages of life.[2] Upon infection, the *Vibrio* spp. pathogen quickly migrates into the digestive gland and damages the hepatopancreatic cells, resulting in shrimp exhibiting clinical signs of anorexia, slow growth, and pale discoloration of the hepatopancreas. A study by de la Peña *et al.* showed that AHPND can lead to sudden death, with a mortality rate of up to 100% within 30–35 days of stocking. The reduction in cellular immune response factors led to a higher mortality of shrimp when challenged with 1 × 10^6 CFU *V. alginolyticus* per mL.[3]

Besides the risk of bacterial disease, high nitrite levels are often seen in intensive and recirculatory aquaculture systems due to the oxidation of ammonia and the incomplete reduction of nitrate. An increase in nitrite concentration beyond the threshold could reduce the blood oxygen-carrying capacity, disrupt the endocrine system, and cause the aquatic animals to weaken and die.[4] Depending on the species, the lethal dose of nitrite can be different. For instance, the LC_{50} of nitrite at 48 h for most of the shrimp species is around 12.1 mM, while the

[a]*Graduate University of Science and Technology, Vietnam Academy of Science and Technology, 18 Hoang Quoc Viet Road, Cau Giay District, Hanoi 100000, Vietnam. E-mail: thuhp@ims.vast.ac.vn*

[b]*Institute of Biotechnology, Vietnam Academy of Science and Technology, 18 Hoang Quoc Viet Road, Cau Giay District, Hanoi 100000, Vietnam*

[c]*Institute of Materials Science, Vietnam Academy of Science and Technology, 18 Hoang Quoc Viet Road, Cau Giay District, Hanoi 100000, Vietnam*

[d]*Vietnam National University of Agriculture, Trau Quy, Gia Lam District, Hanoi 100000, Vietnam*

† Electronic supplementary information (ESI) available. See DOI: https://doi.org/10.1039/d3ra07361k

‡ Both authors contributed equally to this work.

LC_{50} of nitrite at 96 h for the fish larvae is approximately 8.6 mg nitrite per L. Tseng *et al.* also reported that exposure of *L. vannamei* shrimp to 4.94 mgN-NO_2 per L for 96 h significantly decreased total haemocyte count and phenoxidase activity. In addition, NO_2^-, NO_3^-, and PO_4^{3-} ions could induce the growth of pathogens, as multiple studies have suggested that *Vibrio* spp. pathogens can thrive in environments with high concentrations of such inorganic pollutants.[5,6] Therefore, the management of water quality should be based on a combination of methods that simultaneously reduce pollutant levels and pathogen density.

Semiconductor material like TiO_2 is well-known for their broad-spectrum antimicrobial activity and the ability to photodegrade various pollutant compounds.[7] The major antibacterial mechanism of TiO_2 involves the formation of reactive oxygen species (ROS) in the presence of UV light ($\leq$400 nm), hence triggering oxidative stress for bacterial cells.[8] Besides, Ag nanoparticles are often used in antibacterial applications and exhibit a UV-visible absorption maximum in the range of 400–500 nm.[9] Thus, TiO_2 can be modified with silver to reduce the band gap energy of the composite material for easy photoexcitation by visible light and increase the bactericidal effect.[10] A study by Zhang *et al.* showed that the TiO_2–Ag complex had a higher antibacterial activity than the TiO_2 material alone, reaching a sterilization efficiency of over 99.655% against *Escherichia coli*, *Staphylococcus aureus*, *Shigella*, and *Salmonella* when irradiated with visible light for 2 h.[11] Besides, compared to another metal-doped titanium dioxide such as Pt, Pd, Co, Cu, Ni, and Au, the TiO_2–Ag composite also exhibited a higher nitrite removal efficiency of approximately 86% after 3 h of irradiation.[12] However, studies showed that the reduction of nitrite by the photocatalyst can either form N_2 gas or a toxic compound of NH_4^+ compound,[13,14] as presented in reaction (1) and (2):

$$NO_2^- + 8H^+ 6e^- \rightarrow NH_4^+ + 2H_2O \quad (1)$$

$$2NO_2^- + 8H^+ + 6e^- \rightarrow N_2 + 4H_2O \quad (2)$$

$$HNO_2 + H_2O \rightleftarrows H^+ + NO_2^- \quad (3)$$

To produce one molecule of N_2, the presence of two N species is required on the photocatalyst surface, making the ratio of surface coverage of N species to reductant species one of the critical factors controlling the photocatalytic performance. Tugaoen *et al.* suggested that this ratio is largely dependent on the pH of the environment.[14] TiO_2–Ag has a point of zero charge (pH_{pzc}) of approximately 6.6, hence, a solution pH < pH_{pzc} induces protonation and positive charging of the photocatalyst surface.[15] On the other hand, nitrite has a pK_a value of 3.3, indicating a solution pH < pK_a would direct the reaction (3) toward the form of anion NO_2^- instead of HNO_2.[16] Although the neutral molecule, HNO_2, can be adsorbed on the semiconductor surface, the oppositely charged ions would exhibit stronger interaction. Therefore, an acidic pH smaller than pH_{pzc} and pK_a could increase the adsorption of NO_2^- on the photocatalyst surface by creating an electrostatic force and providing a sufficient H^+ source for the complete reduction of NO_2^-.[17] This requirement makes it unrealistic to apply the photocatalysts for aquaculture water treatment since most aquatic species live in an optimal pH range of 7.8 to 8.5.[18]

In the process of nitrite removal, the use of denitrifying bacteria is recommended as an environmentally friendly method.[19] Enzymes such as nitrite reductase, nitrite oxide reductase, and nitrous oxide reductase in denitrifying bacteria can stimulate the conversion of the water-soluble nitrite compound to gaseous forms (NO, N_2O, or N_2), thus completely removing the nitrite pollutant from the aqueous environment.[20] Studies showed that the biofilm-forming characteristic of bacteria is the formation of an extracellular polymer layer, which can protect them from the negative effects of the external environment.[21,22] In addition, biofilm formation is the basis for the easy adhesion of bacteria to the carrier surface.[23] Moreover, the entrapment of bacterial cells in the polymer matrix is a currently developed method to improve the viability of the cells.[24] Thus, using the bacterial properties and protection effect of the polymer layer, the denitrifying bacteria could be combined with TiO_2–Ag to form a remediation agent for simultaneously inhibiting pathogenic bacteria and removing nitrite in aquaculture water. Recently, the study of coupling photocatalyst and biodegradation in wastewater treatment processes showed a positive result of high treatment efficiency and simple operation.[25] However, to the best of our knowledge, there was no known research focus on investigating the combination of denitrifying bacteria and TiO_2–Ag to treat nitrite pollution and inhibit *V. parahaemolyticus* simultaneously.

Therefore, the present study proposes the fabrication of the expanded clay carrier to use as the basic structure supporting the co-immobilization of TiO_2–Ag and denitrifying bacteria. The TiO_2–Ag and denitrifying bacteria were entrapped in a polymer solution and sequentially immobilized on the EC carrier by an electrostatic bond to form a combined remediation agent. The attachment of TiO_2–Ag onto this porous, floatable material would maximize its photocatalysis activity by increasing the exposure to oxygen on the water/air interface as well as improving the reusability of the material.[26] Additionally, the denitrifying bacteria are usually anaerobic, however, some species have been shown that their nitrite reduction process is unaffected by the presence of oxygen.[27,28] Thus, they are capable of growing under aerobic conditions, but in unfavorable conditions, they can stay inside the surface of the EC pores. Nitrite and oxygen compounds can diffuse through the covering polymer layer to reach the bacteria and thus help them perform the nitrite treatment function well. Within the combined material, the TiO_2–Ag plays the main role in inhibiting pathogenic bacteria like *V. parahaemolyticus* while the denitrifying bacteria could effectively remove nitrite pollutants. *In vitro* experiments were carried out to demonstrate the pollution water treatment efficiency of the prepared material. Based on the obtained results, the potential use of this material in treating aquaculture water was discussed.

Experimental

Materials

The kaolinite and rice husks were purchased at a local agricultural region in the South of Hanoi, Vietnam. All the

chemicals used in this study, including $TiCl_4$ (0.09 M in 20% HCl), $NaBH_4$ (99%), $AgNO_3$ (99%), chitosan, alginate were purchased from Sigma-Aldrich (St. Louis, MO, USA). The aerobic denitrifying bacteria, *Bacillus* sp. ST20, *Bacillus* sp. ST26 and pathogenic bacteria *Vibrio parahaemolyticus* were provided by the Environmental Bioremediation Lab, Institute of Biotechnology, VAST. The medium used for denitrifying bacteria culture (D1 medium) consisted of (g L^{-1}): peptone (5), yeast extract (2), meat extract (1), NaCl (5), $NaNO_2$ (0.1), pH 7.5. The basal medium which consisted (g L^{-1}): CH_3COONa (5), K_2HPO_4 (1), and NaCl (5) was used in testing the nitrite removal activity of the synthesized material. *Vibrio parahaemolyticus* was activated in the thiosulfate–citrate–bile salts–sucrose agar plate (TCBS, Sigma-Aldrich, UK), then was aerobically inoculated in the Luria–Bertani medium (LB, Sigma-Aldrich, UK) until reaching a desired bacterial density.[29]

Preparation of expanded clay carrier

The expanded clay (EC) was fabricated from the kaolinite and rice husk by using the pyrolysis process. The kaolinite powder (<2 mm diameter) was mixed with grounded rice husk at a ratio of 1 : 1 (w/w). Water was added to achieve a pliable consistency, making granules about 1 cm in diameter. The granules were dried naturally until a moisture content of 30–40% was reached. Then, they were placed in a furnace at 1200 °C for 2 h and quickly cooled to room temperature using a large ice water bath. This procedure would form numerous holes inside the EC due to the swelling of the molten at high temperatures, and its porosity structure was fixed during the rapid cooling process.[30] Specific surface areas, pore volume, and pore size of the EC samples were determined using N_2 physisorption isotherms at 77 K (Tristar-3030 system, Micromeritics-USA). To initial estimate the Ti and Ag content that existed in the EC carrier, the Inductively coupled plasma mass spectrometry (ICP-MS) analysis of the EC material was carried out utilizing PerkinElmer's Nexion 2000 (USA) equipment.

Synthesis of TiO_2–Ag nanocomposite

TiO_2 nanoparticles were prepared by the precipitation of an aqueous $TiCl_4$ solution with ammonium hydroxide as a precipitation agent.[31] The collected precipitate was washed three times with distilled water by using ultrasonic dispersion to remove impurities, dried at 60 °C for 0.5 h, and heated to 500 °C for 2 h to form the TiO_2NPs. For the synthesis of Ag nanoparticles, 30 mL of $NaBH_4$ 9 mM was used as a reduction agent in 120 mL of $AgNO_3$ 2 mM, then the reaction proceeded for 2 hours under magnetically stirring at 350 rpm. The TiO_2–Ag composite was produced by the method of chemical reduction of silver nanoparticles on the TiO_2NPs surface: 0.4 g of prepared TiO_2NPs were dispersed in 100 mL of distilled water by using an ultrasonic treatment for 5 min, magnetically stirred, and then 5 mL of 0.1 M $NaBH_4$ was added. Dissolving 5 mL of 0.1 M $AgNO_3$ solution into this mixture, it was continuously stirred at 350 rpm for 2 h. Finally, 100 mL of 1% (w/v) sodium alginate was added and stirred at 500 rpm for the next 24 h to form the TiO_2–AgNPs in alginate nanocomposite.

Fourier transform infrared spectroscopy (Shimadzu FTIR Spectrometer 8000 series, SHIMADZU, Japan) was used to analyze the molecular structure of TiO_2–AgNPs in the 400–4000 cm^{-1} wave number range. The crystalline structures of the synthesized nanosystems were examined using a Bruker D8-Advance instrument (Bruker, US) in the reaction mode with a Cu Kα line of 1.5406 Å at 35 kV and 30 mA. At room temperature, data were taken across a 2 range of 30° to 70°, step size of 0.02°, and time per step of 4 s. The Rietveld method was used to assess the detailed structural characterization.

The morphology of the materials was examined using a field emission scanning electron microscope (FESEM; Hitachi S-4800, Japan) and a transmission electron microscopy (TEM; JEOL JEM-1010 system operating at 120 kV). The ICP-MS analysis (ICP Mass Spectrometer, Nexion 2000, PerkinElmer, USA) was used to estimate the ratio of Ag and Ti contents in the TiO_2–Ag composite. The UV-vis spectroscopy analysis was also performed using a UV-6300PC spectrometer (VWR, Radnor PA) to verify the change in optical properties of TiO_2 and TiO_2–Ag composite. The Dynamic Light Scattering (DLS) of the materials were examined with a Malvern Zetasizer Nano ZS (Malvern Instrument, UK) to reveal the nanoparticles size distribution and stability.

Immobilization of TiO_2–AgNPs on expanded clay carrier (nanoparticle/EC)

The EC was immersed in the TiO_2–AgNPs solution and placed in a magnetic stirrer in dark conditions (the ratio of EC particles weight per volume of nanoparticles solution was 1 : 2). During this process, different stirring speeds (0, 250, and 300 rpm) and time (12 and 24 h) were applied. Samples produced in each immobilization condition were collected and used for measuring the concentration of Ti and Ag on EC by the ICP-MS analysis. The material produced was named as TiO_2–Ag/EC. For comparing the antimicrobial activity between TiO_2 and TiO_2–Ag nanoparticles, the TiO_2 immobilized EC (TiO_2/EC) material was additionally fabricated.

Coating nanoparticle/EC with chitosan layer

The TiO_2–Ag/EC was placed onto the chitosan solutions (0.5% (w/v) in 1% acetic acid) for 15 min without stirring before being left to dry at 35 °C for the next 12 h. The formed materials, (TiO_2–Ag)c/EC, were added to the Erlenmeyer flask containing 30 mL of distilled water and rotated at 130 rpm. After 24 h, the content of residual Ti and Ag in EC was measured by the ICP-MS analysis and compared to prior treatment to calculate the detachment rate.

Antibacterial activity of nanoparticle/EC

In this study, the antibacterial activity of the original EC, TiO_2/EC, TiO_2–Ag/EC, and (TiO_2–Ag)c/EC materials against the pathogen *V. parahaemolyticus* and denitrifying bacteria *Bacillus* sp. ST20, *Bacillus* sp. ST26 was evaluated. Briefly, *V. parahaemolyticus* was cultured in LB broth, while *Bacillus* sp. ST20 and *Bacillus* sp. ST26 were grown in D1 broth at 35 °C, 75 rpm for 24 h to reach a bacteria density of 10^8 CFU mL^{-1}. The

bacterial biomass was collected by centrifuging, resuspended in a 0.9% sterilized saline solution, and diluted to obtain a density of 10^6 CFU mL^{-1}. Each bacterial suspension was divided into multiple vials (5 mL per vial). The nanoparticle/EC materials were added to these vials under visible light irradiation by a 400 W halogen lamp (tungsten) for 2 h. The vial containing bacteria suspension without material supplement was used as a negative control. After treatment, the suspension sample was collected to detect bacterial viability. The sample was serially diluted with 0.9% sterilized saline solution and spread (100 μL) into the LB or D1 agar plate and incubated overnight at 35 °C. The number of colony-forming units (CFU mL^{-1}) in the sample was calculated as follows:

Bacteria/mL (CFU mL^{-1}) = (number of the colonies formed on the countable plate × dilution factor)/volume of culture plated in mL

The survival rate of each tested bacteria was calculated by the following equation:

Survival rate (%) = (bacterial density of treated sample/bacterial density of control sample) × 100%

Additionally, the biological characteristics of the bacteria were determined to explain the differential antibacterial activity of the material against the pathogenic and the denitrifying bacteria, in which the Gram identification was carried out based on the method suggested by Gilligan *et al.*,[32] and the biofilm-forming capacity was estimated with the method by Morikawa *et al.*[33]

Immobilization of denitrifying bacteria onto nanoparticles/EC

The denitrifying bacteria, ST20 and ST26, were cultured separately in the D1 broth at 35 °C, 75 rpm for 24 h to reach a bacterial density of approximately 10^8 CFU mL^{-1}, then mixed at a ratio of 1 : 1. Sodium alginate (0.5% w/v) was dispersed into this bacterial mixture at 75 rpm for 2 h to form a homogenous solution. The materials, including original EC, TiO_2–Ag/EC, and (TiO_2–Ag)c/EC were separately immersed in the prepared bacteria suspension and incubated at 35 °C in a static incubator. The original EC served as a positive control to verify the effect of nanoparticles integrated into EC carriers on the bacterial holding capacity of the material. The materials were collected daily for 4 days to determine the effect of the immobilization time on bacterial density and nitrite removal activity. The bacteria-immobilized material was dried at 35 °C for 5 h before being used in the next experiment. The method suggested by Han *et al.* was applied to measure bacterial density in the material.[34] In summary, the material was first shattered into smaller pieces, weighed 0.5 grams, added to 4.5 mL of 0.9% sterilized saline solution, and shaken gently for 15 min. The obtained solution was serially diluted and spread onto the D1 agar plate. After 24 h of incubation at 35 °C, the number of bacteria colonies was counted and used for determining the bacteria colony forming unit per g of EC (CFU g^{-1} of EC).

Nitrite removal efficiency of bacteria-immobilized nanoparticles/EC

The bacteria-immobilized material (weighted approximately 1 g) was added into a 15 mL vial containing 10 mL of basal medium and incubated at 35 °C for 3 days. The initial sodium nitrite concentration was set at 5 mgN-NO_2 per L. The vial containing the material without bacteria immobilized was used as a negative control. The suspension sample from each vial was collected at the beginning, and after 3 days of incubation, centrifuged at 10 000 rpm and used to measure the nitrite concentration by the Griess colorimetric method.[35] The nitrite removal efficiency of the material was calculated by the following equation:

Nitrite removal efficiency (%) = (1 − residual nitrite concentration/initial nitrite concentration) × 100%

Reusability of bacteria immobilized nanoparticle/EC in nitrite removal process

The bacteria-immobilized material was added to the basal medium supplied with 5 mgN-NO_2 per L of sodium nitrite. After 3 days into the treatment of the 1st cycle, the material was collected and then transferred into the fresh medium for another round of treatment (2nd cycle). The experiment continued for six cycles under the same conditions. The nitrite removal efficiency was determined as previously described.

Statistical analysis

All experiments were performed in triplicate. Data were represented as mean ± SD ($n = 3$). The statistical significance was determined by Student's *t*-test, $p < 0.05$ was considered as an indicator of statistical significance.

Results and discussion

Fabrication of expanded clay carrier

In this study, the EC was fabricated simply by the pyrolysis process of kaolinite and rice husk components that are commonly available in Vietnam agricultural areas, thus possibly reducing the synthesis cost. During the fabrication process, the organic matter contained in the rice husk was burned concurrently with the expansion of the kaolinite component at a high temperature of 1200 °C. As a result, these incidents initiated the formation of numerous holes. The size of these holes was later fixed during the rapid cooling step. The EC had a round shape with an average weight of 1.2 ± 0.35 g (Fig. 1a). Brunauer–Emmett–Teller (BET) analysis revealed that this EC material possesses a specific surface area of 4.4 ± 0.12 $m^2\ g^{-1}$ and a pore size of 25.1 ± 0.05 nm with a pore volume around 0.027 ± 0.005 $cm^3\ g^{-1}$. The pore size was consistent with the morphological characteristics observed by FESEM (Fig. 1b). Although, compared to a study by Dutra *et al.*, the prepared EC had a smaller specific surface area than the value of 7.02 $m^2\ g^{-1}$ of the porous clay-based ceramic, the increase in pore size diameter of the prepared EC from 1.84 nm to 25.1 ± 0.05 nm

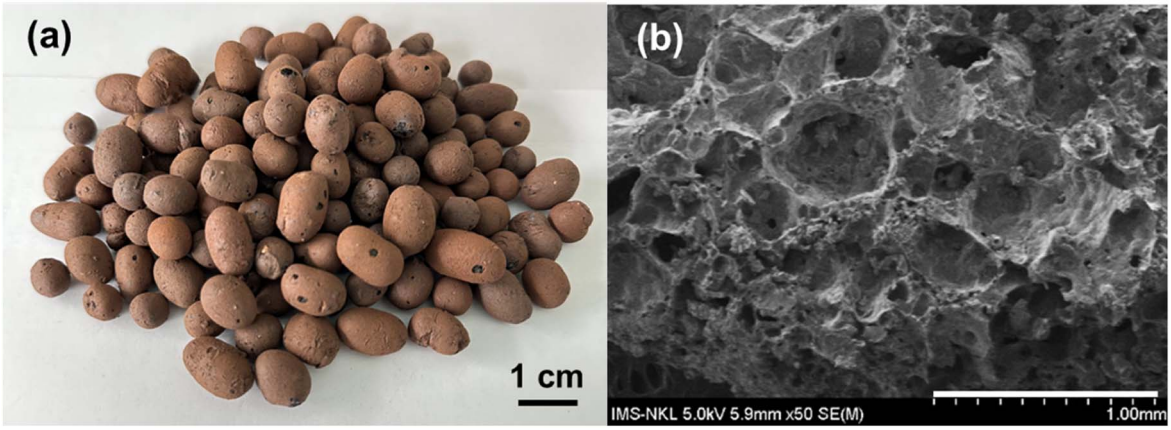

Fig. 1 Appearance (a) and FESEM image (b) of the EC.

was a beneficial characteristic to facilitate the attachment of TiO_2–AgNPs and especially creates favorable conditions for denitrifying bacteria to adhere to the material.[36] The adsorption isotherms (Fig. S1†) demonstrate a type III adsorption shape with a hysteresis loop according to the IUPAC classification of sorption isotherms.[37] The adsorption capacity of EC material was gradually increased with the relative pressure P/P_o, and the adsorption amount ranged from 1.95 to 22.95 g cm^{-3} STP. As the relative pressure exceeds 0.9, the adsorption curves climb extremely quickly, indicating the presence of certain macropores in the EC material.[38]

Preparation of TiO_2–AgNPs

The Ag–TiO_2 nanoparticles were synthesized by the chemical reduction of silver nanoparticles on the TiO_2 surface method. Fig. 2d and e presented the FESEM and TEM images of the synthesized TiO_2–Ag, in which the anchored Ag nanoparticles were seen on the surface of the TiO_2NPs. The Ag could be easily identified as dark spots superimposed on the TiO_2 background due to the significant difference in contrast.[39] The TiO_2 particles were in the size range of 98 ± 11 nm while the anchored Ag particles had a much smaller size of 25.29 ± 3.61 nm (Table S1†).

Fig. 2a shows the FTIR spectra of the TiO_2NPs and prepared TiO_2–AgNPs. From the FTIR spectrum of TiO_2 NPs, the Ti–O vibration band and Ti–O–Ti skeletal frequency may be observed with the strong absorption band at 601 cm^{-1} and 667 cm^{-1}, respectively. These characteristic peaks of Ti–O appeared in the FTIR spectrum of the TiO_2–AgNPs sample but the shift in wave number at 597 cm^{-1} and 652 cm^{-1}, revealed the presence of Ag in the sample and the formation of Ag–TiO_2 bonding.[40–42] Besides, the FTIR spectrum of TiO_2–AgNPs also contained the typical peaks of polymer alginate at 3219 cm^{-1}, 1652 cm^{-1}, and 1338 cm^{-1} corresponding to the valence vibration of –OH (indicate the surface adsorbed OH groups of alginate), C=O, and C–O–C group, respectively.[43] These shifts confirmed the success in the formation of TiO_2–AgNPs.[44,45]

The crystalline phases of TiO_2NPs, AgNPs, and TiO_2–AgNPs were characterized by XRD (Fig. 2b). The XRD pattern of the TiO_2–AgNPs sample displayed characteristic TiO_2NPs peaks located at $2\theta = 25.29°$, 37.85°, 48.06°, 53.91°, 55.11°, 62.6°, and 68.73°, which still matched with the standard card of the anatase phase (JCPDS 78-2486), and was assigned to the (101), (004), (200), and (215) crystallographic planes, respectively. Besides, the peaks located at 2θ values of 38°, 44°, and 64° could be indexed to (111), (200), and (220) diffractions of AgNPs with the face-centered cubic structure (JCPDS 4-0783), respectively.[46] The Ag peaks nearly completely coincided with the TiO_2 anatase phase peaks. As a result, the peaks in TiO_2–AgNPs are similar, indicating that the TiO_2 was efficiently modified with AgNPs. Because of the low concentration of Ag, certain peaks are obscured. These results demonstrated the stable presence of AgNPs in TiO_2–Ag nanocomposite without disrupting the TiO_2 crystal structure.[47–49]

The ICP-MS analysis revealed the Ag content accounted for approximately 4.01 ± 0.09% of TiO_2–Ag composite (Table S1†). In addition, the DLS and SEM analysis showed that the nanoparticles had a uniform granular morphology with an average size of 458.90 ± 18.51 nm, and a zeta potential of −43.70 ± 1.12 mV, which proved the stability of the nanocomposite (Table S1†). The TiO_2–AgNPs were subjected to absorbance measurements in the wavelength range of 300 to 900 nm to verify the change in optical properties of TiO_2 and TiO_2–Ag. In the present study, TiO_2 nanoparticles had maximum absorption at 460 nm and attained a reduced band gap energy (compared to bulk TiO_2) of 2.3 eV (Fig. 2c and S3†). TiO_2–Ag displayed a distinctive absorption peak at 410 nm corresponding to the surface plasmon resonance peak of AgNPs,[46] suggesting that Ag was incorporated to TiO_2–AgNPs, which was consistent with the TEM and SEM results. Interestingly, the introduction of Ag into TiO_2NPs shifted the absorbance threshold of TiO_2–AgNPs into the visible light region, at 700–800 nm, due to the surface plasmon resonance characteristic of the AgNPs. As a result, the TiO_2–AgNPs attained a band gap energy of 2.0 eV (Fig. 2d and S3†).

Immobilization of TiO_2–AgNPs on EC carrier

Initially, the EC contained a low Ti content while the Ag element was not detected (Table 1). Therefore, different stirring speeds and times were tested for their effect on the immobilization

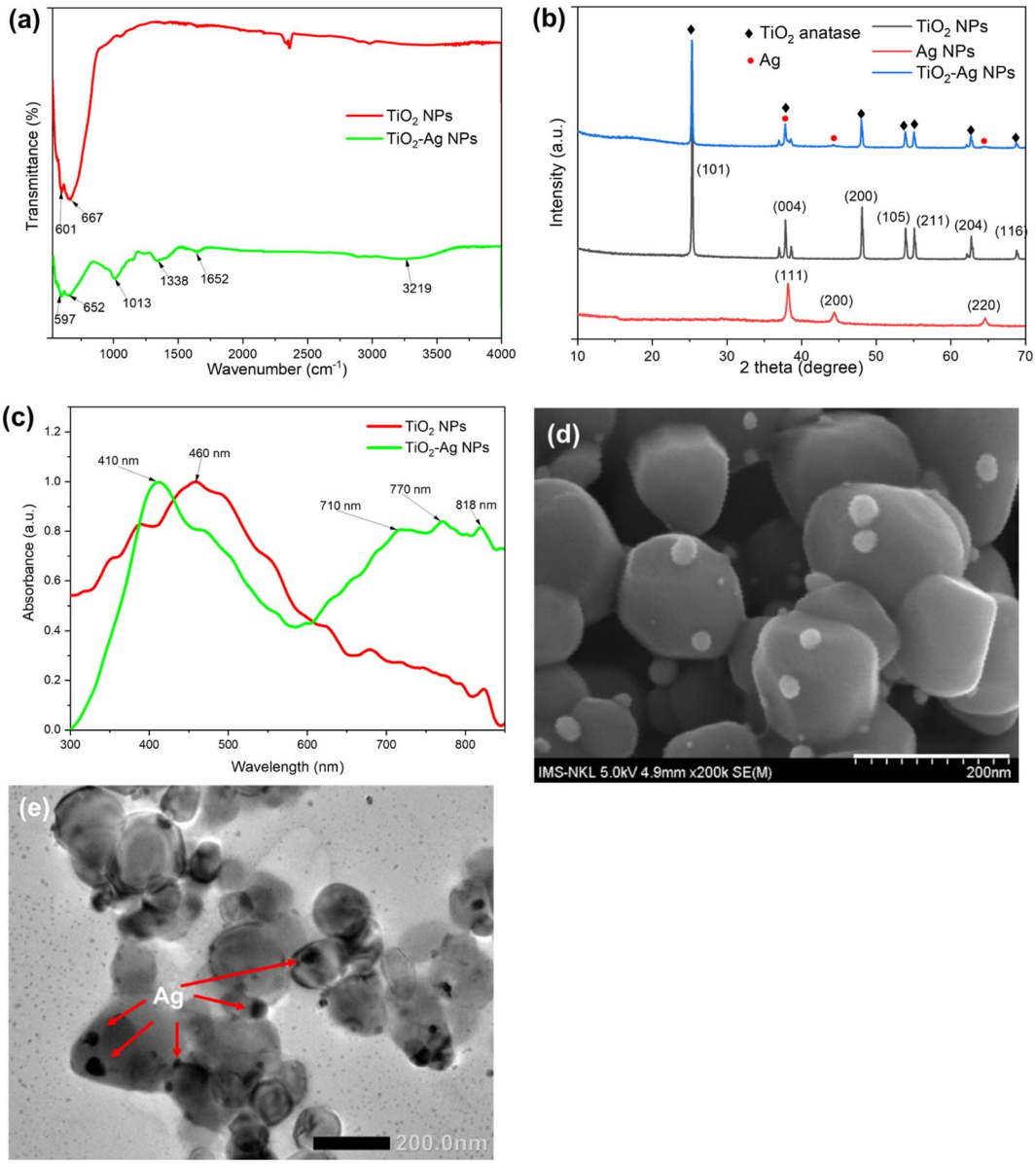

Fig. 2 FTIR spectra (a), X-ray diffractogram patterns (b), UV-Vis absorption spectra (c), FESEM image (d) and TEM image (e) of the TiO_2–Ag nanocomposite.

efficiency of TiO_2–AgNPs on the EC carrier. The results in Table 1 suggested that the increase in stirring speed would reduce the time needed to achieve the highest Ti and Ag concentration immobilized on the EC carrier. Indeed, the highest Ti and Ag contents on EC of 639.38 ± 3.04 and 200.51 ± 3.71 ppm, were achieved after 24 h of stirring at 250 rpm. By increasing the speed to 300 rpm, a comparable amount of Ti and Ag immobilized on EC was also detected after 12 h. However, prolonging the immobilization time at high speed might cause a higher collision between EC carriers and consequently break down the nanoparticles previously attached to the EC surface. Therefore, after 24 h at 300 rpm, the Ti and Ag contents significantly reduced to 220.54 ± 2.64 and 153.57 ± 4.19 ppm, respectively.

To strengthen the stability of the TiO_2–Ag nanoparticles immobilized in the EC carrier, the material, TiO_2–Ag/EC, was coated with a chitosan layer to form the (TiO_2–Ag)c/EC material. As shown in Table 2, the (TiO_2–Ag)c/EC could retain 80.82 ± 0.04% and 79.14 ± 0.002% of its initial Ti, and Ag contents on the material, respectively. On the other hand, without the chitosan layer, only 46.02 ± 0.02 and 36.89 ± 0.47% of the initial Ti and Ag contents were retained after 24 h of treatment (Table 2).

Accessing the antibacterial activity of nanoparticles/EC material

To evaluate the antibacterial activity of the prepared materials against the *V. parahaemolyticus* pathogen, the EC, TiO_2/EC, TiO_2–Ag/EC, and (TiO_2–Ag)c/EC were separately added to the pathogen suspension and irradiated under visible light for 2 h. As shown in Fig. 3a, the viability of *V. parahaemolyticus* was not affected by the TiO_2/EC, the pathogen maintained a survival rate

Table 1 Effect of stiring speeds and times on the immobilization efficiency of TiO_2–AgNPs on EC carrier. nd means not detected

		Ti (ppm)	Ag (ppm)
Original EC		38.94 ± 5.32	nd
Stiring speeds	Times	Ti (ppm) immobilized on EC	Ag (ppm) immobilized on EC
0 rpm	12 h	161.07 ± 1.98	38.73 ± 3.26
0 rpm	24 h	4.54 ± 0.18	52.95 ± 2.04
250 rpm	12 h	508.34 ± 3.86	158.47 ± 2.37
250 rpm	24 h	639.38 ± 3.04	200.51 ± 3.71
300 rpm	12 h	609.17 ± 3.21	261.79 ± 4.39
300 rpm	24 h	220.54 ± 2.64	153.57 ± 4.19

Table 2 Effect of chitosan coating on preventing the detachment of immobilized TiO_2–Ag

Sample	Nanoparticles concentration	Before treatment	After treatment	% nanoparticles remained on EC carrier
Chitosan coated (TiO_2–Ag)/EC	**Ti (ppm)**	647.68 ± 5.96	523.46 ± 4.49	80.82 ± 0.04
	Ag (ppm)	216.19 ± 1.23	171.09 ± 0.98	79.14 ± 0.002
(TiO_2–Ag)/EC without chitosan coating	**Ti (ppm)**	634.87 ± 6.29	342.72 ± 3.23	46.02 ± 0.02
	Ag (ppm)	224.52 ± 4.04	141.67 ± 1.24	36.89 ± 0.47

of 74.8 ± 9.0% (Fig. 4). However, the addition of Ag widened the light absorption spectrum of TiO_2–Ag, leading to higher photocatalytic activity. Therefore, the pathogen was significantly inhibited by the TiO_2–Ag/EC, reducing the survival rate to 28.7 ± 4.5%. The antimicrobial property of chitosan coating in biomedical applications was suggested by a previous study.[50] Thus, the incorporation of chitosan into the TiO_2–Ag/EC further increased the anti-pathogen activity of the material to 99.93 ± 0.1% (Fig. 3a and 4). Moreover, in the present study, when immobilized on a floating carrier, the TiO_2–Ag could easily interact with a high oxygen concentration in the air which induced the continued production of reactive oxygen species. Hence, this advanced property could contribute to the enhanced antibacterial activity of the (TiO_2–Ag)c/EC material. In another study, Yerli-Soylu *et al.* also reported a 99.99% reduction of *E. coli* density by using TiO_2 nanocomposite ceramics doped with AgNPs, but still, irradiation under UV light for 1 h was required in their experiment.[51] Thus, the present study has successfully fabricated a photocatalyst material with high antibacterial activity under visible light irritation.

Interestingly, under similar experiment conditions, the denitrifying bacteria, *Bacillus* sp. ST 20 and ST26 strains, could resist the (TiO_2–Ag)c/EC treatment and showed a survival rate of 95.70 ± 3.26% and 12.60 ± 8.22%, respectively (Fig. 3 and 4). In general, biofilm-producing bacteria show a remarkable resistance capacity to antibiotics and other antibacterial agents like ROS.[52] Within the microenvironment, the penetration of these substances was slowed, while the bacteria cell could differentiate into other forms like the spore to protect the integrity of the cell.[53] In addition, the presence of peptidoglycan in the bacterial cell walls is considered one of the defense barriers under stress conditions.[54] However, these two key antibiotic resistance mechanisms were not found in the Gram-negative *V. parahaemolyticus* pathogen (Fig. S4†). As a result, the *V. parahaemolyticus* pathogen was more susceptible to (TiO_2–Ag)c/EC treatment than other tested bacteria. Although *Bacillus* sp. ST26 belonged to the Gram-negative group, the bacteria have higher biofilm-forming activity compared to *V. parahaemolyticus*, hence ST26 strain partly resisted the (TiO_2–Ag)c/EC treatment. In particular, *Bacillus* sp. ST20 belonged to the Gram-positive group, whose cell wall consists of a thicker peptidoglycan layer than Gram-negative ones, and exhibited the highest capacity for biofilm formation among all the tested bacteria (Fig. S4†). Therefore, these advantageous properties could protect *Bacillus* sp. ST20 and ST26 against the photocatalytic activity of the (TiO_2–Ag)c/EC.

Immobilization of denitrifying bacteria onto nanoparticles/EC and its nitrite removal activity

The two denitrifying bacteria, *Bacillus* sp. ST20 and *Bacillus* sp. ST26, was previously reported as having excellent nitrite removal activity, reaching an efficiency of 95% after 72 h under oxic condition.[27] Besides, these two nitrite-reducing bacteria belonging to the genus *Bacillus* are facultative anaerobic bacteria, meaning they are adapted to grow in a low-oxygen environment. Therefore, the adhesion to EC materials will create favorable conditions for their metabolic activity. A culture of mixed-strain bacteria often enhances their overall biological activity.[55] Therefore, the ST20 and ST26 strains were both chosen to be immobilized on TiO_2–Ag/EC and (TiO_2–Ag)c/EC in order to evaluate their nitrite removal activity. In this study, to increase the immobilization efficiency and protect the denitrifying bacteria from the reactive species produced by TiO_2–Ag, the bacteria biomass was embedded in an alginate

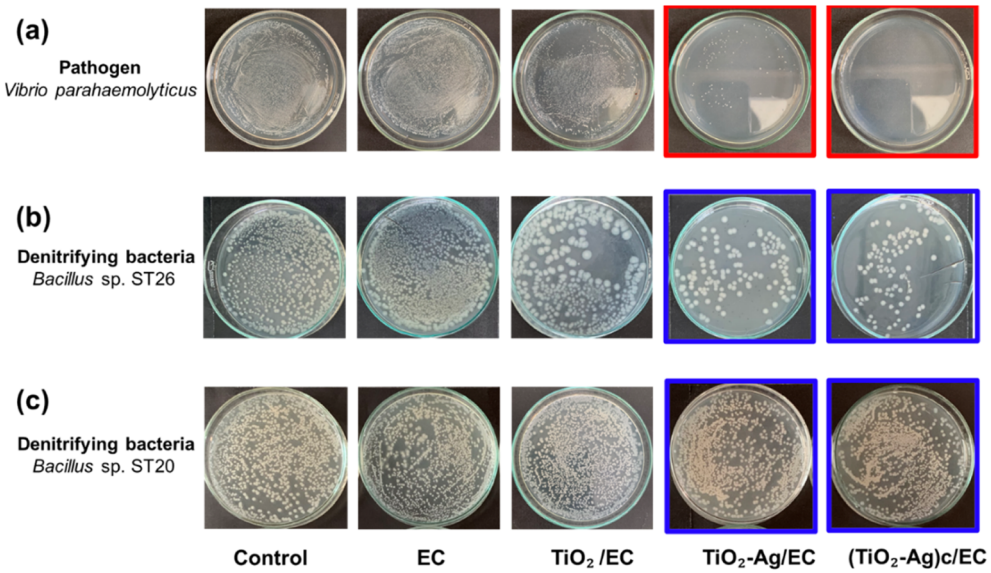

Fig. 3 Differential of antibacterial activity of the synthesized photocatalytic agents against *V. parahaemolyticus* pathogen (a), denitrifying *Bacillus* sp. ST20 (b) and denitrifying *Bacillus* sp. ST26 (c). The control was the bacteria suspension without adding photocatalyst material while the EC symbol indicated the treatment in which bacteria suspension was treated with original EC material (without photocatalyst immobilized).

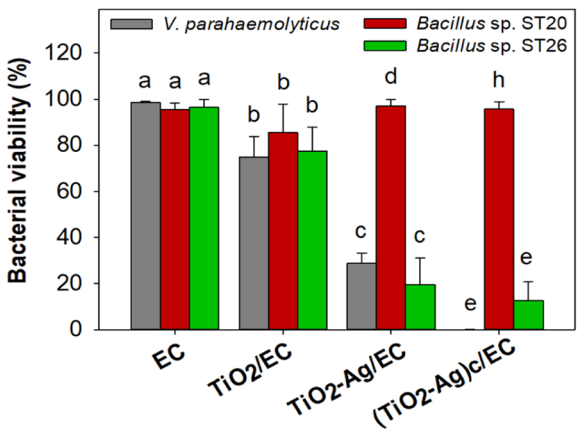

Fig. 4 Bacterial viability when treated with different photocatalytic agents. The statistically different was defined as follow: different letter indicated $p < 0.05$ between viability of each bacteria strain in the same treatment.

solution before immobilizing on (TiO_2–Ag)c/EC material. To take advantage of the oppositely charged between alginate and chitosan, the chitosan layer on (TiO_2–Ag)c/EC material could act as an intermediate layer to enhance the immobilization efficiency of the denitrifying bacteria on the prepared (TiO_2–Ag)c/EC material by creating the electrostatic force between these two components.

The data depicted in Fig. 5 revealed that the biofilm formed by *Bacillus* sp. ST20 and *Bacillus* sp. ST26 matured on day 4th and started to decay on day 5. Based on this observation, the immobilization of these bacteria on the EC, TiO_2–Ag/EC, and (TiO_2–Ag)c/EC materials was carried out by incubating the materials in bacteria suspension for 4 days. The daily variation in the density of immobilized bacteria was depicted in Fig. 5c, in which the counted cell number increased along with the incubation time. The highest bacteria density for all three materials was recorded on day 4th. However, there was a significant difference in bacteria-holding capacity between these materials ($p < 0.05$). On day 4th, the highest bacteria density of $(76.67 \pm 9.43) \times 10^7$ CFU g^{-1} was detected on (TiO_2–Ag)c/EC, followed by $(33.33 \pm 4.71) \times 10^7$ CFU g^{-1} in TiO_2–Ag/EC and 5.0×10^7 CFU g^{-1} in the EC (Fig. 5c). These results proved that in the process of immobilizing TiO_2–Ag, the existence of the electrostatic bond between chitosan and alginate could enhance the attraction of bacteria cells to the surface of (TiO_2–Ag)c/EC compared to TiO_2–Ag/EC. The FESEM images showed denitrifying bacteria cells remained intact when incorporated in (TiO_2–Ag)c/EC material. The fuzzy layer around the cell might indicate the formation of a bacterial biofilm (Fig. 5a and b).

As shown in Fig. 5d, the nitrite-reducing activity was also well performed by the bacteria-immobilized TiO_2–Ag/EC and (TiO_2–Ag)c/EC material, reached a removal efficacy of 92.5 to 95.5%, which was statistically higher than the activity of the EC material of $80.3 \pm 3.8\%$. These results demonstrated that the presence of TiO_2–Ag did not significantly affect the growth as well as nitrite reduction activity of the denitrifying bacteria.

Reusability of bacteria immobilized nanoparticle/EC in the nitrite removal process

Fig. 6 presented the reusability of denitrifying bacteria immobilized on nanoparticle/EC materials. After three days, a high removal efficiency of 94.96 ± 1.66 to $98.60 \pm 0.34\%$ was measured for all three materials. Nevertheless, the nitrite reduction activity of TiO_2–Ag/EC and EC gradually decreased as the materials were recycled repeatedly. In the fourth cycle, (TiO_2–Ag)c/EC could remove $98.20 \pm 0.11\%$ of the initial nitrite

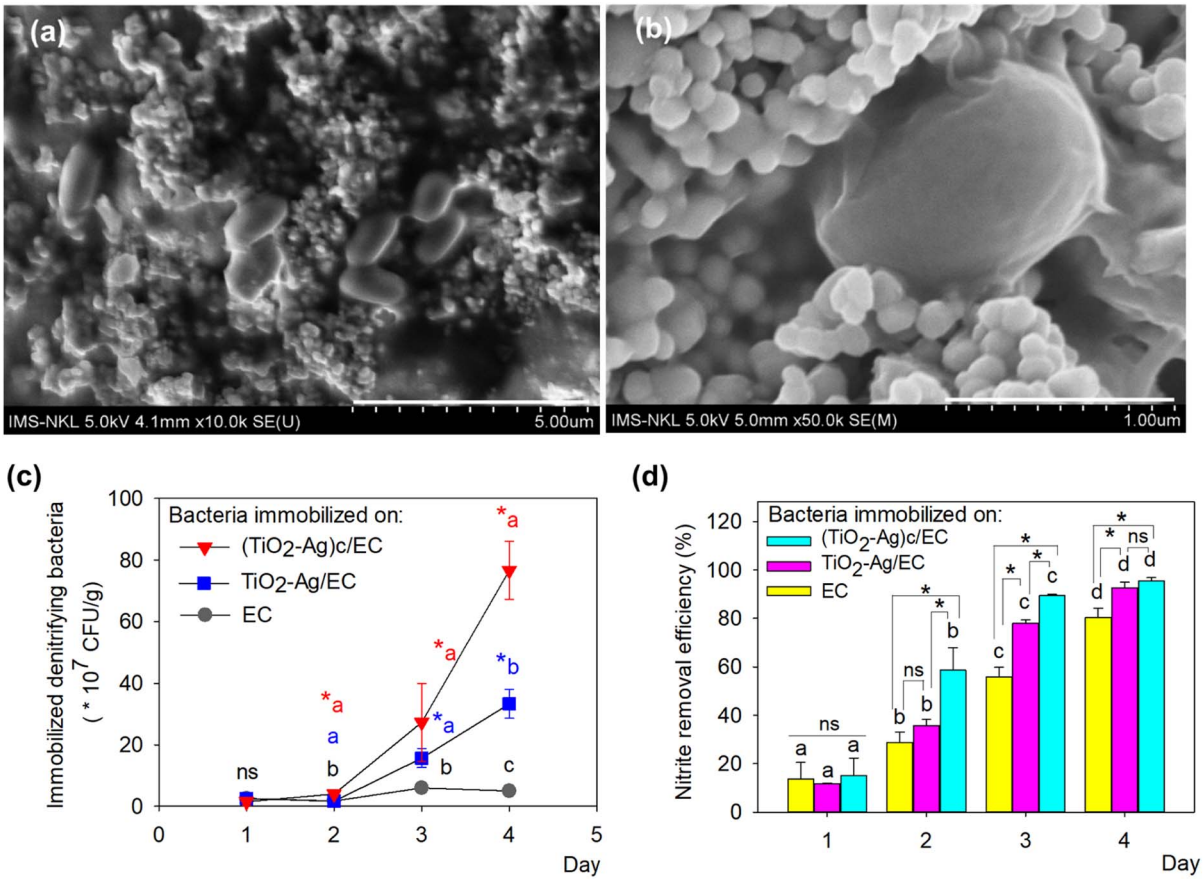

Fig. 5 FESEM images (a and b) of the denitrifying bacteria immobilized on (TiO_2–Ag)c/EC material; bacteria density (c) and nitrite removal efficiency (d) of bacteria immobilized on various materials at different times. The statistically different was defined as follow: for panel (c), the asterisk symbol (*) indicated $p < 0.05$ of a material at different times, while different letter showed $p < 0.05$ between three types of material at the same sampling times; and *vice versa* for the panel (d).

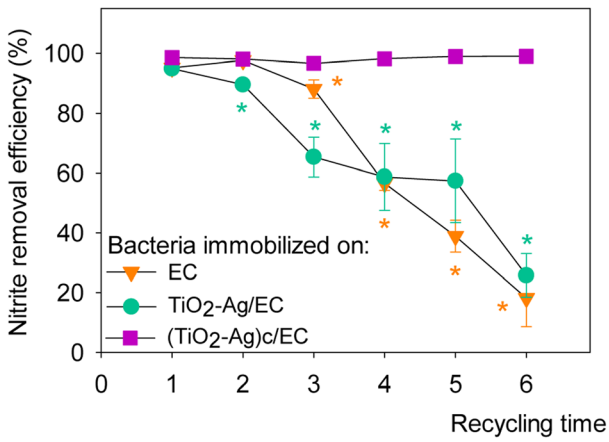

Fig. 6 Reusability of denitrifying bacteria immobilized on different synthesized materials. The asterisk symbol (*) indicated $p < 0.05$ between different recycling times of material.

concentration, while the removal efficiency of TiO_2–Ag/EC and EC decreased to less than 60%. In contrast, (TiO_2–Ag)c/EC maintained its nitrite removal activity as high as 99.0 ± 0.27% in cycle 6th. This value was not significantly different compared to the first cycle, indicating a highly reusable property of the material. Therefore, a further study could investigate the applicability of this combined material in the aquafarming field.

Conclusions

Herein, we first presented the evidence of intimate coupling between denitrifying bacteria and the TiO_2–Ag in a floating expanded clay carrier (EC) to co-treat nitrite pollution and inhibit the growth of *V. parahaemolyticus* pathogen. The EC carriers exhibiting porosity and floatable properties were fabricated through the pyrolysis process. The modification of TiO_2NPs with Ag reduced the band gap energy of TiO_2–AgNPs to 2 eV. The optimization process of immobilizing TiO_2–Ag on EC showed that the increase in stirring speed would reduce the time needed to achieve the highest Ti and Ag concentration immobilized on the EC carrier. Applying the stirring speed of 250 rpm, the content of Ti, and Ag immobilized on the EC carrier reached the highest values of 639.38 ± 3.04 ppm and 200.51 ± 3.71 ppm, respectively. To minimize the detachment level of TiO_2–Ag from EC, the material was then coated with a chitosan (0.5%) layer. Interestingly, the presence of the

chitosan component increased the anti-*V. parahaemolyticus* activity of the synthesized material to approximately 99%, while having no significant impact on the viability of denitrifying bacteria and their nitrite removal activity. Therefore, the denitrifying bacteria were immobilized on (TiO_2–Ag)c/EC material, demonstrating a stable nitrite removal efficiency of 99.0 ± 0.27% after six reuses. In this study, the successful simultaneous immobilization of a photocatalyst and denitrification of bacteria is due to the knowledge of the characteristics of the bacteria and the role of the photocatalyst. Based on the presented results, the fabricated bacteria immobilized (TiO_2–Ag)c/EC material is suggested as a potential remediate agent for aquaculture water treatment.

Author contributions

Phuong Ha Hoang, Minh Thi Nguyen: investigation; formal analysis; writing – original draft. Ke Son Phan, Huong Giang Bui: methodology; writing – review & editing. Thi Thu Huong Le, Nhat Huy Chu, Ngoc Anh Ho, Quang Huy Pham and Xuan Khoi Tran: conceptualization; methodology, writing – review & editing. Phuong Ha Hoang, Phuong Thu Ha: conceptualization; writing – review & editing; funding acquisition; supervision.

Conflicts of interest

There are no conflicts to declare.

Acknowledgements

This work is financially supported by The Ministry of Agriculture and Rural Development of Vietnam (Grant No. 03/HĐ-KHCN). Minh Thi Nguyen was funded by Vingroup JSC and supported by the Master, PhD Scholarship Programme of Vingroup Innovation Foundation (VINIF), Institute of Big Data, code VINIF.2022.TS075.

Notes and references

1 M. A. Hassan, N. A. Abd Allah and M. Mabrok, *Aquaculture*, 2021, **536**, 736447.
2 V. Kumar, S. Roy, B. K. Behera, P. Bossier and B. K. Das, *Toxins*, 2021, **13**(8), 524.
3 I. T. Tseng and J. C. Chen, *Fish Shellfish Immunol.*, 2004, **17**, 325–333.
4 A. Ciji and M. S. Akhtar, *Rev. Aquacult.*, 2020, **12**, 878–908.
5 R. M. Atlas, A. Horowitz, M. Krichevsky and A. K. Bej, *Microb. Ecol.*, 1991, **22**, 249–256.
6 H. H. Sung, H. C. Li, F. M. Tsai, Y. Y. Ting and W. L. Chao, *J. Exp. Mar. Biol. Ecol.*, 1999, **236**, 261–271.
7 S. J. Armaković, M. M. Savanović and S. Armaković, *Catal*, 2023, **13**, 26.
8 M. Ozdal and S. Gurkok, *ADMET DMPK*, 2022, **10**, 115.
9 J. M. Ashraf, M. A. Ansari, H. M. Khan, M. A. Alzohairy and I. Choi, *Sci. Rep.*, 2016, **6**, 20414.
10 H. Liu, X. Dong, C. Duan, X. Su and Z. Zhu, *Ceram. Int.*, 2013, **39**, 8789–8795.
11 Y. Zhang, X. Zhao, S. Fu, X. Lv, Q. He, Y. Li, F. Ji and X. Xu, *Ceram. Int.*, 2022, **48**, 4897–4903.
12 H. Kominami, A. Furusho, S. Y. Murakami, H. Inoue, Y. Kera and B. Ohtani, *Catal. Lett.*, 2001, **76**, 31–34.
13 F. Zhang, Y. Pi, J. Cui, Y. Yang, X. Zhang and N. Guan, *J. Phys. Chem. C*, 2007, **111**, 3756–3761.
14 H. O. N. Tugaoen, S. Garcia-Segura, K. Hristovski and P. Westerhoff, *Sci. Total Environ.*, 2017, **599–600**, 1524–1551.
15 L. Gomathi Devi and K. Mohan Reddy, *Appl. Surf. Sci.*, 2010, **256**, 3116–3121.
16 H. Duan, S. Gao, X. Li, N. H. Ab Hamid, G. Jiang, M. Zheng, X. Bai, P. L. Bond, X. Lu, M. M. Chislett, S. Hu, L. Ye and Z. Yuan, *Water Res.*, 2020, **171**, 115382.
17 M. Pavel, C. Anastasescu, R. N. State, A. Vasile, F. Papa and I. Balint, *Catalysis*, 2023, **13**, 380.
18 W. N. Wang, A. L. Wang, L. Chen, Y. Liu and R. Y. Sun, *Aquat. Toxicol.*, 2002, **60**, 75–83.
19 J. Zhang, C. Fan, M. Zhao, Z. Wang, S. Jiang, Z. Jin, K. Bei, X. Zheng, S. Wu, P. Lin and H. Miu, *Chemosphere*, 2023, **313**, 137474.
20 L. Philippot, *Biochim. Biophys. Acta, Gene Struct. Expression*, 2002, **1577**, 355–376.
21 K. U. Mahto, Vandana, M. Priyadarshanee, D. P. Samantaray and S. Das, *J. Cleaner Prod.*, 2022, **379**, 134759.
22 W. Yin, Y. Wang, L. Liu and J. He, *Int. J. Mol. Sci.*, 2019, **20**(14), 3423.
23 A. Dzionek, D. Wojcieszyńska, K. Hupert-Kocurek, M. Adamczyk-Habrajska and U. Guzik, *Catal*, 2018, **8**, 176.
24 J. C. Bassani, V. A. Queiroz Santos, A. M. Barbosa-Dekker, R. F. H. Dekker, M. A. A. da Cunha and E. A. Pereira, *LWT–Food Sci. Technol.*, 2019, **102**, 411–417.
25 L. Zhang, Y. Zhang, K. Xiao, J. Shi, X. Du, L. Wang and X. Wu, *New J. Chem.*, 2021, **45**, 13029–13039.
26 M. Sboui, H. Lachheb, S. Bouattour, M. Gruttadauria, V. La Parola, L. F. Liotta and S. Boufi, *Environ. Res.*, 2021, **198**, 111257.
27 P. H. Hoang, T. M. Nguyen, N. C. T. Le, K. S. Phan, T. T. T. Mai and P. T. Ha, *Curr. Microbiol.*, 2022, **79**, 209.
28 M. Deng, Z. Dai, Y. Senbati, L. Li, K. Song and X. He, *Front. Microbiol.*, 2020, **11**, 544066.
29 T. L. A. Pham, Q. K. Le, T. T. Nguyen, N. P. C. Do and T. T. H. Nguyen, *IFMBE Proceedings*, 2020, vol. 69, pp. 681–684.
30 T. M. Nguyen, P. T. Ha, T. T. H. Le, K. S. Phan, T. N. C. Le, T. T. T. Mai and P. H. Hoang, *J. Biosci. Bioeng.*, 2022, **134**(1), 41–47.
31 W. Buraso, V. Lachom, P. Siriya and P. Laokul, *Mater. Res. Express*, 2018, **5**, 115003.
32 P. H. Gilligan, *The Prokaryotes: Human Microbiology*, 2013, pp. 57–89.
33 M. Morikawa, S. Kagihiro, M. Haruki, K. Takano, S. Branda, R. Kolter and S. Kanaya, *Microbiology*, 2006, **152**, 2801–2807.
34 S. Han, I. Jang, E. K. Choi, W. Park, C. Yi and N. Chung, *J. Environ. Eng.*, 2020, **146**, 04020072.
35 N. S. Bryan and M. B. Grisham, *Free Radicals Biol. Med.*, 2007, **43**, 645.

36 L. F. Dutra, M. E. Freitas, A. C. Grillet, N. Mendes and M. Woloszyn, *Materials*, 2019, **12**(6), 946.
37 K. A. Cychosz and M. Thommes, *Engineering*, 2018, **4**, 559–566.
38 D. Jeong, S. C. Kim, T. An, D. Lee, H. Hwang, S. Q. Choi and J. Park, *Nanomaterials*, 2023, **13**(16), 2351.
39 D. Guin, S. V. Manorama, J. N. L. Latha and S. Singh, *J. Phys. Chem. C*, 2007, **111**, 13393–13397.
40 E. H. Alsharaeh, T. Bora, A. Soliman, F. Ahmed, G. Bharath, M. G. Ghoniem, K. M. Abu-Salah and J. Dutta, *Catalysis*, 2017, **7**, 133.
41 T. Dayakar, K. V. Rao, M. Vinodkumar, K. Bikshalu, B. Chakradhar and K. R. Rao, *Appl. Surf. Sci.*, 2018, **435**, 216–224.
42 L. Gharibshahi, E. Saion, E. Gharibshahi, A. H. Shaari and K. A. Matori, *Materials*, 2017, **10**, 402.
43 K. Son Phan, T. Thu Huong Le, T. Minh Nguyen, T. Thu Trang Mai, P. Ha Hoang, X. Thang To, T. Trung Nguyen, K. Dang Pham and P. Thu Ha, *ChemistrySelect*, 2022, **7**, e202201954.
44 Z. D. Mahmoudabadi, E. Eslami and M. Narimisa, *J. Colloid Interface Sci.*, 2018, **529**, 538–546.
45 G. Yang, Z. Jiang, H. Shi, T. Xiao and Z. Yan, *J. Mater. Chem.*, 2010, **20**, 5301–5309.
46 K. S. Phan, T. M. Nguyen, X. T. To, T. T. H. Le, T. T. Nguyen, K. D. Pham, P. H. Hoang, T. N. Dong, D. K. Dang, T. H. T. Phan, T. T. T. Mai and P. T. Ha, *RSC Adv.*, 2022, **12**, 35730–35743.
47 T. Narkbuakaew and P. Sujaridworakun, *Opt. Mater.*, 2019, **98**, 109407.
48 M. Michalska, J. Pavlovský, K. Lemański, M. Małecka, M. Ptak, V. Novák, M. Kormunda and V. Matějka, *Mater. Today Chem.*, 2022, **26**, 101123.
49 H. Chakhtouna, H. Benzeid, N. Zari, A. el kacem Qaiss and R. Bouhfid, *Environ. Sci. Pollut. Res. Int.*, 2021, **28**, 44638.
50 A. Guarnieri, M. Triunfo, C. Scieuzo, D. Ianniciello, E. Tafi, T. Hahn, S. Zibek, R. Salvia, A. De Bonis and P. Falabella, *Sci. Rep.*, 2022, **12**, 1–12.
51 N. Yerli-Soylu, A. Akturk, Ö. Kabak, M. Erol-Taygun, F. Karbancioglu-Guler and S. Küçükbayrak, *Int. J. Eng. Sci. Technol.*, 2022, **35**, 101175.
52 C. Uruén, G. Chopo-Escuin, J. Tommassen, R. C. Mainar-Jaime and J. Arenas, *Antibiotics*, 2021, **10**, 1–36.
53 D. Sharma, L. Misba and A. U. Khan, *Antimicrob. Resist. Infect. Control*, 2019, **8**, 1–10.
54 A. K. Yadav, A. Espaillat and F. Cava, *Front. Microbiol.*, 2018, **9**, 2064.
55 P. Puvanasundram, C. M. Chong, S. Sabri, M. S. Yusoff and M. Karim, *Aquac. Rep.*, 2021, **21**, 100905.